Noname manuscript No.
(will be inserted by the editor)

Slingshot spiders build tensed underdamped webs for ultrafast launches and speedy halts

Elio J. Challita* · Symone Alexander* · Sarah Han · Todd A. Blackledge · Jonathan A. Coddington · Sunghwan Jung · M. Saad Bhamla

arXiv:2103.05756v1 [physics.bio-ph] 7 Mar 2021

Received: date / Accepted: date

Abstract We develop a mathematical model to capture the web dynamics of slingshot spiders (Araneae: Theridiosomatidae), which utilize a tension line to deform their orb webs into conical springs to hunt flying insects. Slingshot spiders are characterized by their ultrafast launch speeds and accelerations (exceeding 1300 m/s^2), however a theoretical approach to characterize the underlying spatiotemporal web dynamics remains missing. To address this knowledge gap, we develop a 2D-coupled damped oscillator model of the web. Our model reveals three key insights into the dynamics of slingshot motion. First, the tension line plays a dual role: enabling the spider to load elastic energy into the web for a quick launch (in milliseconds) to displacements of 10-15 body lengths, but also enabling the spider to halt quickly, attenuating inertial oscillations. Second, the dominant energy dissipation mechanism is viscous drag by the silk lines - acting as a low Reynolds number parachute. Third, the web exhibits underdamped oscillatory dynamics through a finely-tuned balance between the radial line forces, the tension line force and viscous drag dissipation. Together, our work suggests that the conical geometry and tension-line enables the slingshot web to act as both an elastic spring and a shock absorber, for the multi-functional roles of risky predation and self-preservation.

Keywords Ray orbweavers · Theridiosomatidae · Underdamped oscillator · Spider biomechanics · Arachnid locomotion

Introduction

The sit and wait strategy of many orb-weaving spiders is well known for the ability to effectively snare prey using sticky silk and the rapid dissipation of the captured prey's kinetic energy (Das et al., 2017; Kelly

*These authors contributed equally

Elio J. Challita
Chemical and Biomolecular Engineering, Georgia Institute of Technology, Atlanta, GA 30311, USA
Mechanical Engineering, Georgia Institute of Technology, Atlanta, GA 30311, USA

Symone Alexander
Chemical and Biomolecular Engineering, Georgia Institute of Technology, Atlanta, GA 30311, USA

Sarah Han
Department of Biology, Integrated Bioscience Program, The University of Akron, Akron, OH 44325 , USA

Todd A. Blackledge
Department of Biology, Integrated Bioscience Program, The University of Akron, Akron, OH 44325, USA

Jonathan A. Coddington
Smithsonian Institution, National Museum of Natural History, 10th and Constitution, NW Washington, DC 20560, USA

Sunghwan Jung
Department of Biological and Environmental Engineering, Cornell University, Ithaca, NY 14853, USA

M. Saad Bhamla
Chemical and Biomolecular Engineering, Georgia Institute of Technology, Atlanta, GA 30311, USA
E-mail: saadb@chbe.gatech.edu

et al., 2011; Sensenig et al., 2012; Yu et al., 2015). Slingshot spiders, orb-weavers known for extending and releasing their webs like slingshots to capture prey, evolved an orb web modified with a tension line attached at its central hub (Alexander and Bhamla, 2020; Alves et al., 2007; Coddington, 1986, 2005; Eberhard, 1981, 1986, 1990; Hingston, 1932; Wienskoski, 2010). The tension line enables the spider to deform its web into a 3-D conical structure, loading elastic energy into the radial lines that ultimately facilitates rapid accelerations ($> 1300\ m/s^2$) for capturing flying prey (SI Movie 1), or possibly avoiding predation (Alves et al., 2007). Although in previous work, we described how the slingshot spider loads the web as a spring to achieve ultrafast motion (Alexander and Bhamla, 2020), it remains unclear how the spider leverages its unique web and tension line to decelerate quickly and come to a halt, either after successful capture or missing of prey (Eberhard, 1990), and to reset its web to potentially fire again. What are the relevant physical forces governing energy storage and energy dissipation in the web? How does the conical geometry affect the slingshot spatial and temporal dynamics? The role of the tension line in enabling the spider to load energy into the web as a spring is known, but what role does the tension play in stopping the spider's motion? To address these open questions, we develop a mathematical model of the slingshot spider web dynamics in this paper.

The slingshot spider grips the center of its web with four rear legs while incrementally pulling and twisting the tension line and coiling the silk with claws on its anterior legs and pedipalps (non-locomotor anterior appendages) to store elastic energy in the radial lines of the web (Fig. 1a) (Alexander and Bhamla, 2020; Coddington, 1986). Upon sensing external stimuli (for example a finger snap), the spider releases the tension line, catapulting both the web and spider backwards (Fig. 1b). Multiple trajectories ($n = 5$) are provided in Fig. 1c, with the full displacement taking place in around 30 ms. The dominant movement is mostly in the y-direction (10 - 15 mm or 10-15 $\times$ body lengths) with smaller movements ($\pm$1.1 mm, less than one body length) in the x-direction. Spiders achieve vertical speed of up to 4.2 m/s ($v_{max} = 4.16 \pm 0.07\ m/s$) and accelerations exceeding 1300 m/s^2 ($a_{max} = 1163 \pm 144\ m/s^2$) (Alexander and Bhamla, 2020). Despite this ultrafast millisecond motion, we observe that the resultant vibrational response of the web attenuates within milliseconds as well - suggesting that the web design facilitates both energy storage and speed as well as energy dissipation, which could potentially improve prey capture, reduce the probability of damage to spider or web, and/or facilitate rapid reset and reloading of the web.

Motivated by the rapid attenuation of the slingshot spiders motion as well as its non-planar configuration, we set to theoretically model the dynamics of the slingshot spider web. We treat the slingshot motion like the dynamic response of a step input typically used in process control design (Kuo, 1987). Specifically, we focus on spatiotemporal parameters such as the rise time, overshoot and settling time. Modeling the forces in the radial lines and the tension line allows us to explore how they enable both rapid movement and quick return back to the equilibrium position. The mathematical model described herein offers insights about the balance of elastic forces in slingshot spider webs and the opportunity to understand their design in ways that are difficult to achieve experimentally.

Methods

Field Videography

Field work was conducted in Puerto Maldonado, Peru at the Tambopata Research Center ($-13.134°$, $-069.609°$). Research permit no. 654-2018-GOREMAD-GRRNYGMA-DRFFS was obtained by the Gerencia Regional Forestal y de Fauna Silvestre. The spiders were located by scanning dead branches and leafy plants for their conical webs and then snapping fingers near to the web to confirm slingshot motion. A Chronos 1.4 high speed camera (Krontech) was utilized for high speed video recording (up to 38,500 fps) in conjunction with a field portable Zaila high intensity light with portable battery packs. Field Videos were captured at 1057 fps.

Field specimen and silk collection

The spider specimen was identified to the best of our ability as an undescribed species in the genus *Epeirotypus* sp. (Araneae: Theridiosomatidae) (see SI text for images of organism including epigynum). Videography was performed utilizing spiders that had built webs in their natural habitat. After observation

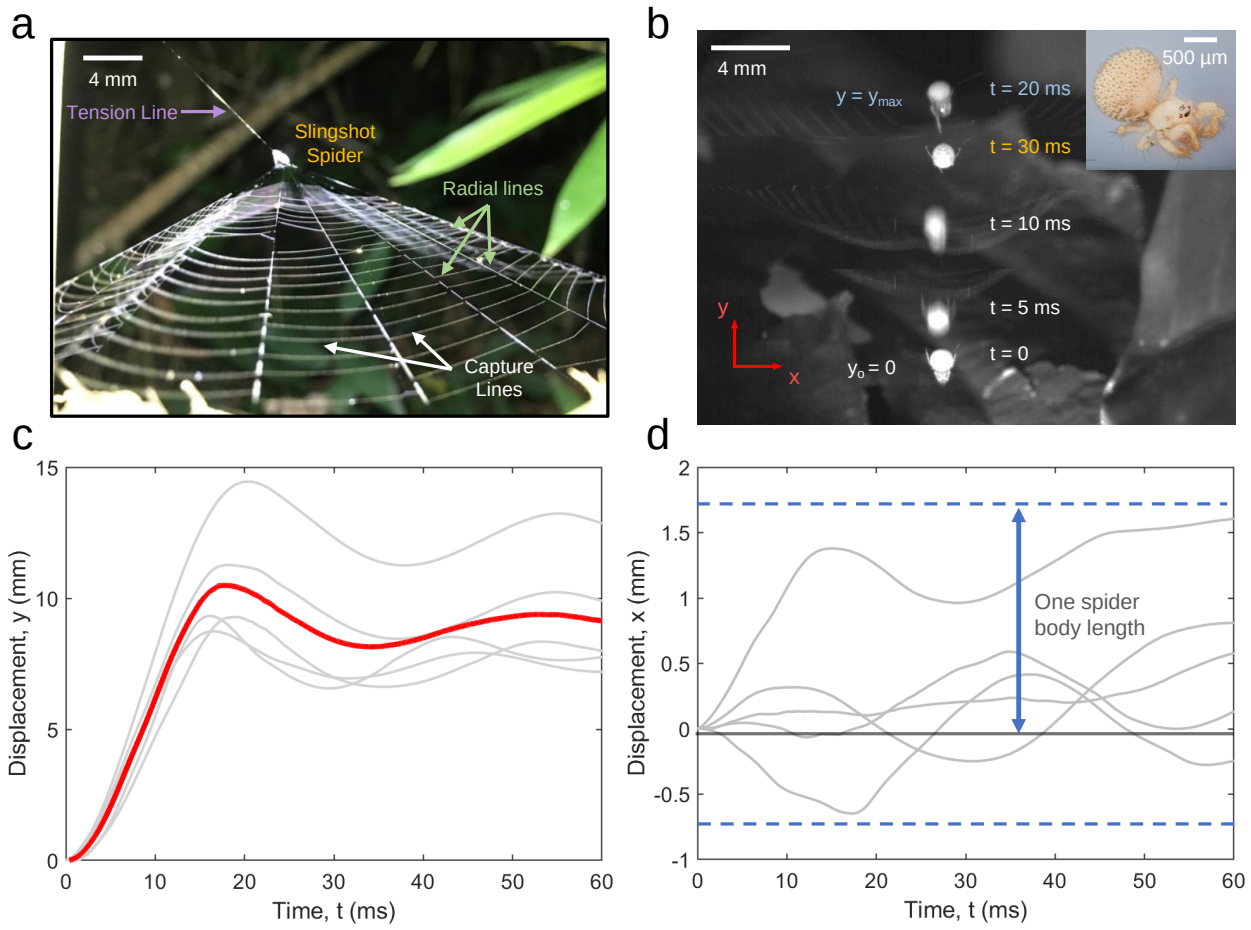


Fig. 1: **Slingshot spider web dynamics**. **a** The spider loads elastic energy by pulling on the tension line, thereby stretching the radial lines and deforming the web and forming a conical web structure. The spider remains in this position awaiting its prey. We note from field observations that the spider web does not seem to have a specific preference for orientation with respect to gravity. **b** Upon sensing a stimulus the slingshot spider releases the web moving explosively, almost 9 times its body length in less than 30 ms. The web is oriented horizontally with the tension line at the bottom of the frame, so that the primary motion upon release in the positive y direction facing upwards in this case. **c** Quantification of the multiple trajectories of the same single slingshot spider for repeated launches (triggered by snapping fingers). The red line denotes the average trajectory of the multiples displacement curves. We adjust trajectories so that they all start at $(x = 0, y = 0)$ at $t = 0$. **d** Movement in the x direction is negligible before the first oscillation.

and videography, spider specimens were collected and stored in 200 proof ethanol for species identification and further analysis. Silk samples were collected using a notched microscope slide.

High speed video analysis

Matlab was employed to analyze the highspeed video obtained in the field. The code was written to identify the spider in each frame using an intensity threshold and record the location of its centroid. Accurate tracking was verified utilizing a binary output video highlighting the spider as white and setting the background as black. The code converted the units of the centroid measurements from pixels to meters and calculated elapsed time from the frame rate and number of frames to calculate displacement, velocity, and acceleration.

Mathematical Model

We mathematically model the spatiotemporal dynamics of the motion of the slingshot spider as a 2D mass-spring model in x-y direction (Fig. 2a). The model consists of three springs: two symmetric springs extended in the radial/horizontal x direction ($F_{r1,2}$) and one in the vertical y direction that represents the tension line (F_t). We model the spider as a point mass (m_s) located at the intersection of the three springs (Fig. 2). In the following subsections, we describe different components of the model in detail along with relevant assumptions and limitations.

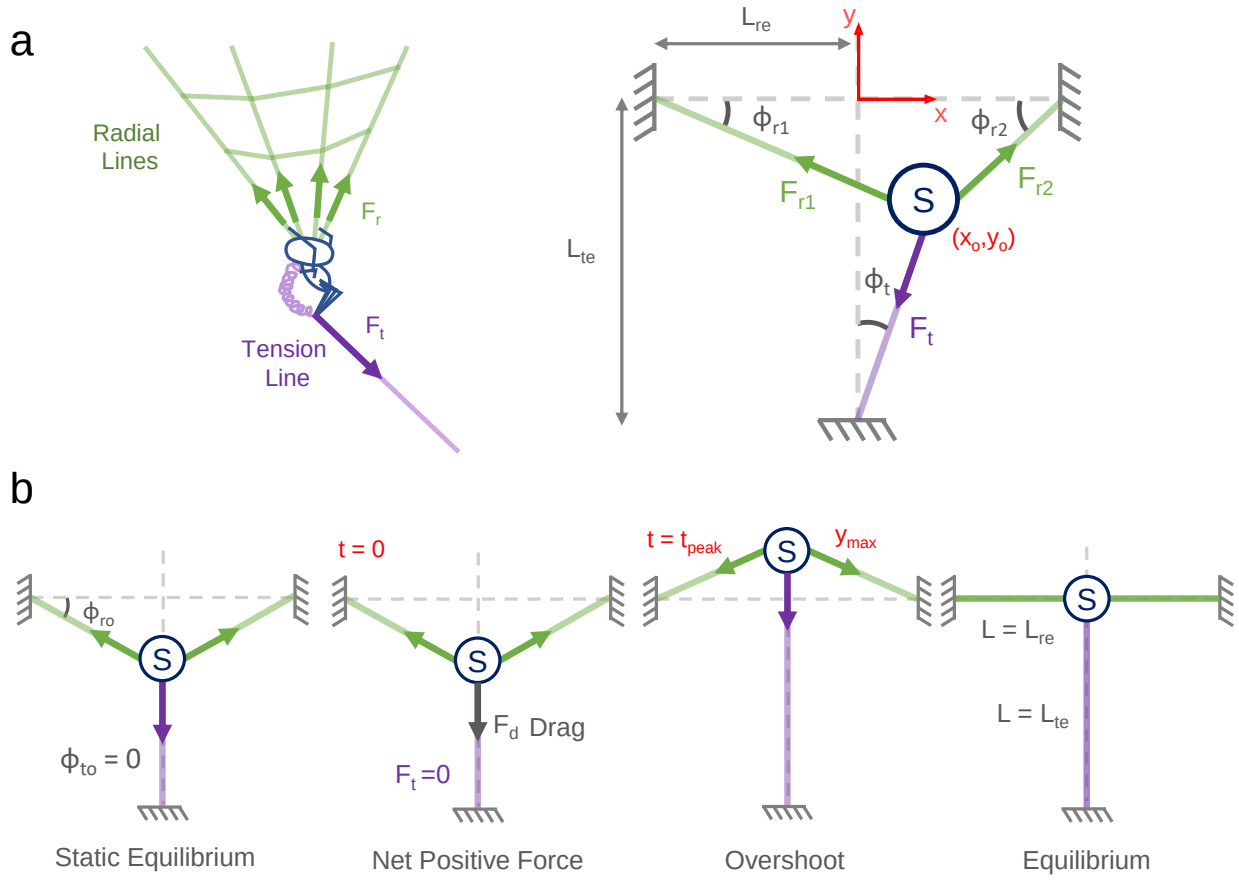


Fig. 2: **Schematic of the mathematical model. a** We model the conical web structure as two symmetric horizontal radial springs and a vertical tension line located in a 2D plane. We assume that the slingshot spider is a point mass having a characteristic length D_s on the order of $\sim 1.3\ mm$ located at the intersection of radial lines and the tension line. We define $L_{r,eq}$ and $L_{t,eq}$ as the equilibrium length of the the radial lines and the tension line respectively.The spider starts at (x_o, y_o) at $t = 0$. Each force has a projected component in the x and y directions. Our model ignores the effects of gravity on the slingshot dynamics and the positive y direction is set facing the upward direction. **b** We consider the case of a pure 1D motion where at $t < 0$, the radial lines forces are balanced by the tension line force. At $t = 0$, the spider releases the tension resulting in a net force in the positive (upward in this particular case) y-direction caused by the radial lines and opposed by the air drag. When the spider crosses the equilibrium point, the tension line starts stretching, resulting in a restoring downward force. The spider continues oscillating, while slowly approaching equilibrium.

2D web geometry

We define ϕ_{r1} and ϕ_{r2} as the angles formed between the radial lines and the x-axis and ϕ_t as the angle between the tension line and the y-axis (Fig. 2b). We prescribe two equilibrium points to the model (Fig. 2b). The first equilibrium point is before the spider launches ($t < 0$, $\phi_{r1,2} = \phi_{r0}$, Fig. 2c), when the spider has deformed the web into a cone and waits for a prey to come within striking distance. At this point the forces in the radial springs are balanced by the force in the tension line and the system is in a static equilibrium. The second equilibrium point is defined when the all the web lines (radial and tension line) are at their equilibrium lengths (L_r=$L_{r,eq}$, L_t=$L_{t,eq}$, $\phi_{r1,2} = \phi_t = 0$, Fig. 2c). This point occurs when the spider's motion has ceased and all the web forces are equal to zero (Fig. 2c). We note that in the actual slingshot spider web these equilibrium points may be shifted due to the asymmetric architecture of the web. However for the purposes of our model, this assumption is valid as we are assuming that the springs are linear and that the variations in the forces are more important to the dynamics compared to the absolute base forces themselves. In a sense, this is similar to the treatment of a vertical mass-spring system where the effects of gravity are ignored since the equilibrium point is defined when the weight is balanced by the initial extension of the spring.

Elastic silk springs

We make two assumptions to model the silk web lines (radial and tension lines) as elastic force-generating springs. First, the silk lines are approximated as linear Hookean springs ($F = K \cdot \Delta L$) with no internal viscous damping. We recognize that this assumption is a significant simplification since actual silk fibers behave as complex and nonlinear viscoelastic materials (Gosline et al., 1984, 1986; Kelly et al., 2011; Tietsch et al., 2016; Yu et al., 2015). The spring constant K is defined by $K = EA/L_{eq}$, where A is the cross-sectional area of the silk measured using SEM images (See SI text Fig. 4), and L_{eq} is the equilibrium length and E is the silk's young modulus. The silk's young modulus ranges between $\sim 1 - 10$ GPa and is obtained from the nonlinear stress-strain curves of the major ampullate (MA) silk of various spider species (Gosline et al., 1999; Ko et al., 2011) .

Second, unlike conventional springs that can exert a push or pull force depending on compression or extension, our modeled silk springs react only to extension to exert a pulling force - they cannot push (Jung et al., 2014). Mathematically, we incorporate this through the Heaviside function $\Theta(\Delta L)$, which is defined as $\Theta(\Delta L) = 1$ when the silk spring is extended ($\Delta L > 0$) and $\Theta(\Delta L) = 0$ for compression $\Delta L < 0$.

Energy dissipation to the environment through aerial drag

The energy of the system is dissipated by viscous drag to the environment by the fast moving spider and web. We ignore any friction that might arise between the spider pedipalps. Viscous damping in the silk lines itself is also ignored as discussed earlier. The aerodynamic drag of an object traveling through a fluid (air) depends on several factors such as its geometry, dimensions and flow conditions. The Reynolds number, which determines the effect of inertial forces with respect to viscous forces, is typically calculated to identify the type of damping involved in the system. The Reynolds number is estimated as $Re = \rho\ V_{max}\mathrm{D}/\mu$, where ρ= 1.225 kg/m^3 is the density of air, V_{max} is the spider speed, D is the characteristic length and μ =1.81×10^{-5} kg/(m s) is the viscosity of air. The Reynolds number is calculated for both the spider and the web below.

The characteristic length of the spider is estimated to be $D_s \sim$ 1.75 mm (fig. 2a) yielding a $Re_s \sim$ 280. The spider drag is approximated by flow around a sphere at finite Reynolds number as $F_{d,s} = C_s V_s^2$, where $C_s = \frac{1}{2} C_d A_s \rho_{air}$, $C_d \sim 1.25$ is the drag coefficient at $Re \sim 280$ and $A_s = \frac{\pi}{4} D_s^2$ is the characteristic cross-sectional area, and V_s is the spider instantaneous speed (Vogel, 2009).

Since the silk fibers are orders of magnitude smaller than the spider itself, we expect the Reynolds number for the silk to be much lower. Assuming each silk line as a cylinder that pivots around a stationary substrate so that the web moves at half the speed as the spider ($V_w = V_s/2$), we obtain a Reynolds number $Re_w \sim$ 0.1. For these low Reynolds numbers, we can estimate the drag on the silk lines using slender body theory

in Stoke flows (Gary Leal, 2007) as: $F_{dw} = \frac{4\pi L_w \mu V_w}{ln\frac{L_w}{D_w}}$, where L_w and D_w are the web length and diameter, respectively (see Table 1). Due to the principle of linearity in low Reynolds flow, we can add up the drag contributions from all the radial and capture lines by measuring them and summing up the drag forces. A summary of the values used in the model are provided in Table 1.

		Simulation 1	**Simulation 2**	
	Parameter	**Value**	**Value**	**Source**
Spider	Mass, m_s (Kg)	1.6×10^{-3}	1.6×10^{-3}	Measured
	Characteristic Length, D_s (m)	1.3×10^{-3}	1.3×10^{-3}	Measured
	Body Length, BL (m)	1.75×10^{-3}	1.75×10^{-3}	Measured
	Damping coefficient, C_s (Kg/s)	8.3×10^{-7}	8.3×10^{-7}	Calculated
Radial lines	Number, N_r	8	8	Field Data
	Young's Modulus, E_r (Pa)	0.35×10^{10}	0.45×10^{10}	(Gosline et al., 1999)
	Diameter, D_r (m)	1×10^{-6}	1×10^{-6}	SEM
	Length, L_r (m)	4.5×10^{-2}	4.5×10^{-2}	Measured
	Equilibrium Length, $L_{r,eq}$ (m)	2.34×10^{-2}	2.34×10^{-2}	Measured
Tension line	Young's Modulus, E_t (Pa)	0.35×10^{10}	0.45×10^{10}	(Gosline et al., 1999)
	Diameter, D_t (m)	1×10^{-6}	1×10^{-6}	SEM
	Length, L_t (m)	4×10^{-2}	4×10^{-2}	Measured
	Equilibrium Length, $L_{t,eq}$ (m)	6×10^{-2}	6×10^{-2}	Measured
Capture lines	Number per radial line	13	13	Measured
	Length, L_c (m)	6.5×10^{-3}	6.5×10^{-3}	Calculated
Total web lines	Total Length, L_w (m)	1.03	1.03	Calculated
	Damping coefficient, C_w (Kg/s)	2.41×10^{-4}	2.41×10^{-4}	Calculated
Initial Conditions	x_o (m)	-4.5×10^{-4}	-18.5×10^{-4}	
	y_o (m)	-12×10^{-3}	-12×10^{-3}	

Table 1: **Simulation parameters and their values.** Summary of the geometrical parameters and physical properties used in the simulation. The source of these parameters is either from literature or measure from field data. The results of simulations 1 and 2 are shown in Fig. 4a and Fig. 5a, respectively.

2-D Equations of Motion

Considering all the forces (inertia, web elasticity, and drag) along x and y directions, we write the 2D equations of motion that describe the trajectory of the slingshot spider as a function of time as follows:

$$\begin{aligned} \textbf{x-axis} &: m_s\ddot{x} = -F_{r1x} + F_{r2x} - F_{tx} - F_{dsx} - F_{dwx} \\ \textbf{y-axis} &: m_s\ddot{y} = -F_{r1y} - F_{r2y} - F_{ty} - F_{dsy} - F_{dwy} \end{aligned} \tag{1}$$

where:

$$F_{r1,2x} = \Delta L_{r1,2}\ K_r\ \cos\phi_{r1,2}\ ,\ F_{r1,2y} = \Delta L_{r1,2}\ K_r\ \sin\phi_{r1,2}$$

$$F_{tx} = \Delta L_t\ K_t\ \sin\phi_t\ ,\ F_{ty} = \Delta L_t\ K_t\ \cos\phi_t$$

$$F_{dwx} = C_w\ \frac{\dot{x_s}}{2}\ ,\ F_{dwy} = C_w\ \frac{\dot{y_s}}{2}$$

$$F_{dsx} = C_s\ \ (\dot{x_s}^2 + \dot{y_s}^2)\cos(\arctan\frac{\dot{y_s}}{\dot{x_s}}),\ F_{dsy} = C_s\ (\dot{x_s}^2 + \dot{y_s}^2)\sin(\arctan\frac{\dot{y_s}}{\dot{x_s}})$$

$$\Delta L_{r1,2} = L_{r1,2} - L_{r,eq}\ ,\ L_{r1,2} = \sqrt{L_{r,eq1,2}^2 \pm x^2} - L_{r,eq1,2}$$

$$\sin\phi_{r1,2} = \frac{y}{L_{r1,2}}\ ,\ \cos\phi_{r1,2} = \frac{L_{r,eq1,2} \pm x}{L_{r1,2}}\ ,\ \sin\phi_t = \frac{x}{L_t}$$

$$K_{r1,2} = \frac{E_{rA_r}}{L_{r,eq1,2}}\ ,\ K_{t1,2} = \frac{E_{tA_t}}{L_{t,eq1,2}}$$

At $t < 0$, the spider is at static equilibrium at a position (x_o,y_o) where the radial spring forces ($F_{r1,2}$) are opposed by the force (F_t) exerted by the tension line (Fig. 2c1). At $t = 0$, the tension force is set to zero resulting in a net upward motion. This is akin to the spider launching itself when triggered by an external stimulus. The x-y trajectories are obtained by numerically solving the equations (1) and (2) using the 4th order Runge-Kutta approach in Matlab. The system starts from static equilibrium at (x_o,y_o) at $t = 0$. The simulation is stopped after 200 ms has elapsed.

Results and Discussion

Web dynamics in 1D motion

To understand the dynamics of the system, we first consider the limiting 1D case, where the motion is purely in the y-direction ($\phi_t = 0\ ,\ x = 0\ ,\ \forall t\ $) (Fig. 2c). This assumption may be valid during the initial stages of the motion, where the displacement is almost one-dimensional in the y-direction and relatively negligible in other dimensions (Fig. 1c-d). However, this assumption breaks down during the later stages of the displacement as motion gets more complex. Nevertheless, this approach helps to shed light on several key features of the slingshot motion as well as providing guidance to the iterative exercises of fitting the model to the data.

We assess the goodness of the fit by using four different spatiotemporal parameters: peak time (t_p, ms), settle time (t_s, ms), overshoot (%), and rise time (t_r, ms), which are graphically defined in Fig. 3. The peak time is duration that the spider takes to go from initial position to the maximum displacement y_{max}. The overshoot is the percentage offset the spider travels with respect the equilibrium point $\frac{y_{max}-y_{eq}}{y_{eq}}$. The settling time ($t_s$) is the duration that the spider take to go from the initial peak displacement to the first oscillatory peak that falls between $\pm$ on the body length (BL) above the equilibrium point. We assume that at this point, the slingshot motion has practically come to a halt and the spider is able to reset the elastic loading.

The rise time t_s corresponds to the time the spider takes to go from $y = y_o$ to $y = y_{eq}$ during the first oscillation (Fig. 3). During this time $t < t_s$, the spatiotemporal dynamics are mainly governed by the radial line forces F_r along with drag F_d, while the tension line force F_t is zero ($\Delta L_t < 0$). The initial rise time is $t_s = 2\pi/\omega_{d,n}$ where $\omega_{d,n}$ is the damped natural frequency. Once $\Delta L_t \geq 0$, the tension line becomes engaged and the restoring force F_t starts influencing the dynamics of the system. Specifically, the damped natural frequency becomes proportional to the combined effect of both the radial lines and the tension line ($\omega_n \propto (K_r + K_t)^{\frac{1}{2}}$ when $y > y_{eq}$).

The mass subsequently oscillates around the equilibrium point with diminishing amplitudes before eventually stopping as the kinetic and potential energies get dissipated by drag. An interesting geometrical feature of the model is that as the mass approaches the equilibrium point ($y \to 0$, $\phi \to 0$), the projected radial forces in the y direction drop sharply.

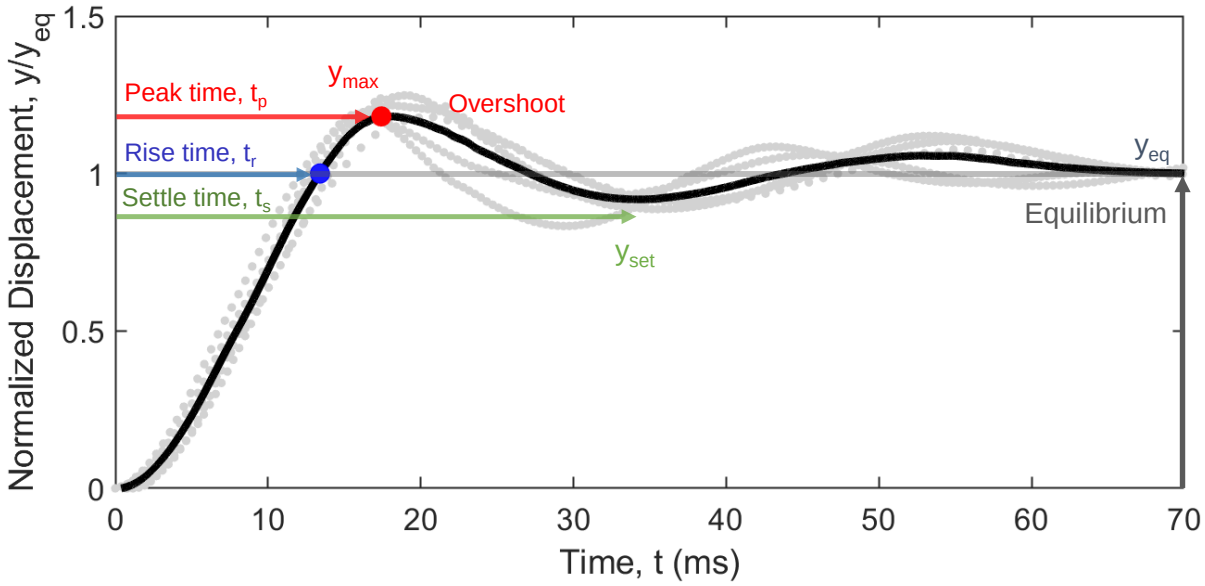


Fig. 3: **Defining key parameters of slingshot spider trajectories.** We focus on several spatial and temporal parameter to assess the fit between the mathematical model and the field data. The equilibrium point is set as the final displacement (y_{eq}) when the spider comes to a halt. We define the rise time (t_s) as the duration from $y = 0$ to the first time the spider cross the equilibrium point (y_{eq}) and the peak time (t_p) is the time taken to reach the maximum displacement (y_{max}). We measure the overshoot as the ratio between the max displacement and the equilibrium point ($\frac{y_{max}-y_{eq}}{y_{eq}}$). These variables are highlighted here on the average normalized displacements ($n = 5$) in the vertical direction of a single slingshot spider. Finally, we define the settling time as the time it takes the spider to finish one oscillation with an amplitude that falls between $\pm$ one body length of the spider.

Slingshot Dynamics in a 2D motion

Next, we solve the equations of motion in 2D while changing the physical and geometrical parameters to better fit the displacement of the spider. To avoid major variations in geometry and initial conditions, we validate the simulation outputs with multiple firing events ($n = 5$) of a single spider (Fig. 1b-d). By matching the initial conditions of the model (x_o, y_o) to the experimental data, we show the output of the model in Fig. 4a, referred to as Simulation 1. The model captures the rise time, peak time and maximum peak with less than 5% error as quantified in Table 2. However, the model does not accurately capture the secondary oscillations ($t > 30$ ms), and also predicts a $\sim$ 20 ms longer setting time compared to experimental observations. In the x-direction, the model captures both the amplitudes and frequency of the oscillations with a phase shift, as seen qualitatively with the x-y map (Fig. 4d).

The temporal evolution of the underlying forces is also computed and highlighted in conjunction with the y-displacement. The radial forces projected into the y-direction start with a combined maximum value of around $\sim 7.5{\times}10^{-4}$ N or 75 dynes. Interestingly, this falls within the force ranges previously measured in the radial silk lines of slingshot spider webs using a custom-built tension apparatus by Coddington (Coddington, 1986). The net radial forces in the x-direction are relatively smaller and become more significant at $t > 30$ ms as the spider approaches equilibrium. The tension line force F_t is only enabled when $\Delta L_t > L_{t,eq}$, and is observed as a sharp increase in the negative direction (retarding spider motion) around $t =$ 14 ms (Fig. 4b). The drag forces in the y-direction start from zero and rapidly increase in magnitude as the spider approaches

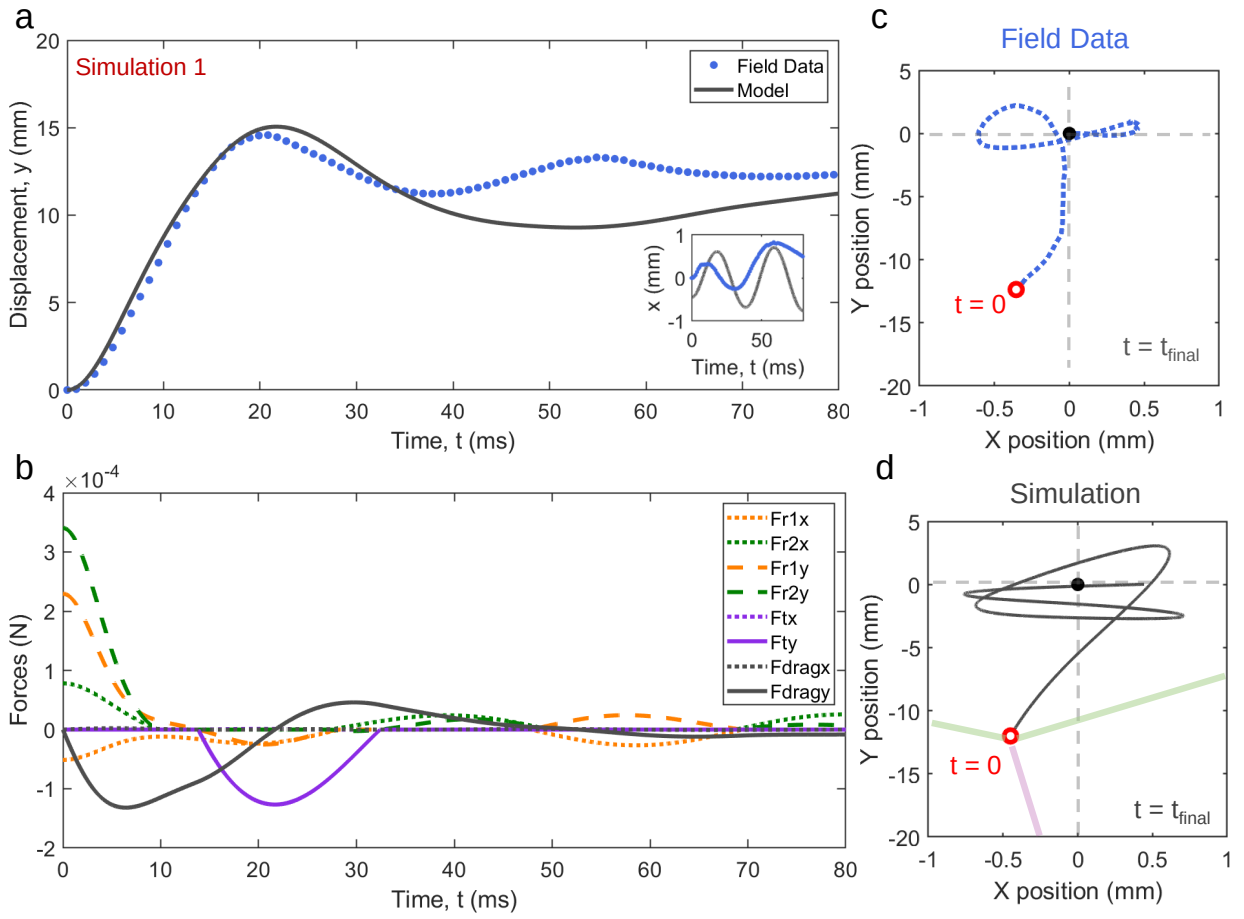


Fig. 4: **Simulation 1: Slingshot spider dynamics in 2-D. a** We obtain the x-y displacement of the spider by solving the equations of motion (Eq. 1). The simulation output matches the rise time, maximum peak and maximum output y_{max}, as well the minimal oscillations in the x direction. However, beyond the first fluctuation, the model does not predict any subsequent oscillations in the y-direction. **b** The temporal evolution of the forces reveals that the system starts with forces in the radial lines in the x-y directions. As the system picks up speed, drag from the web resists the motion - drag from spider is negligible. The restoring force in the tension line which has been zero so far, steps in as the tension line becomes stretched ($t \sim 15\ ms$). **c,d** The simulation also predicts the apparent 2D displacement of the spider starting from from (x_o, y_o) at $t = 0$. The simulation show a qualitatively similar trajectory in the x-y plane, as the spider initially catapults in the y-direction before undergoing low amplitude oscillations in the x-direction as it slowly approaches equilibrium.

$V_{s,max}$ before decreasing as the mass comes to a halt. We note that the radial web forces and drag forces are always acting in opposite directions - the web forces driving motion and drag damping it.

Two underlying assumptions made in this model are that the trajectory of the slingshot spider is confined in a 2D plane and that the spider behaves as a point mass object. In reality, the slingshot motion is a more complex 3D motion, but we only record a projection of the motion in 2D with a single high-speed camera in the field. Moreover, the mass of the spider is not equally distributed (asymmetric body) with most of its mass not facing the tension line. This unequal distribution of mass causes the spider to behave like a 3D inverted pendulum that can rotate around the point of intersection between the spider and the silk (as seen in SI Movie 1) (Han et al., 2019). The model also ignores any displacement biases that might arise due to asymmetries in the web structure, since the spider constructs the web in small plant branches. To highlight the consequences of displacement biases in an orthogonal direction (z direction), we consider an exaggerated

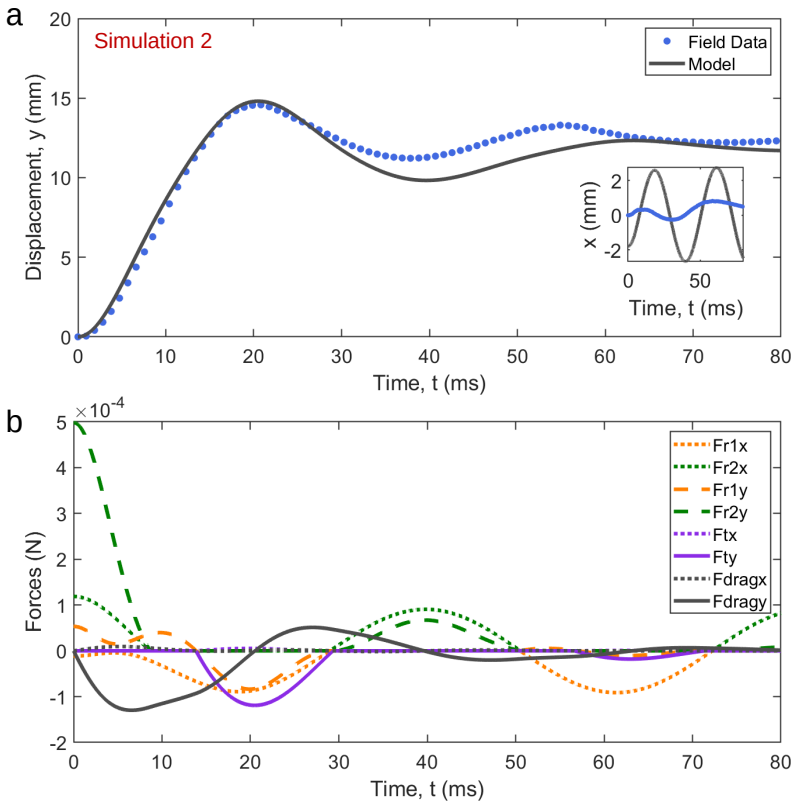


Fig. 5: **Simulation 2 with larger contributions from x-motion. a** To capture the dynamics of the subsequent vibrations in the y-direction, we run a second simulation with an exaggerated initial displacement in the x-direction (4 $\times$ the one used in simulation 1). This highlights the additional layer of complexity imposed by an amplified orthogonal motion. The model matches the field data better in terms of the temporal parameters as well as the subsequent low amplitude fluctuations after the first overshoot. In reality, the spider motion is 3D, which may include twisting and rotation due to asymmetries in mass and geometry (See SI Movie 1). These extraneous influences become more significant at low amplitudes and frequencies. **b** The evolution of the forces in the $x-y$ plane show similar dynamics as seen earlier in Fig. 4b. Interestingly, the tension force in the x-direction becomes more pronounced here as the influence in the x-direction is amplified due to the initial conditions.

case in the initial value of x where we run the simulation after multiplying x_0 by 4. The results shown in Fig. 4 show better agreement between the model and field data, and the secondary oscillations in the experimental data are matched well by the model, including matching of the settling time (Table 2).

In summary, despite the major dimensional reductions assumed in developing this simplified mathematical model, our model still captures salient spatiotemporal dynamic features that arise due to the complex design of the slingshot spider web. The values used in the model fall within the biological boundaries in terms of physical properties and geometrical constraints (Tables 1,2). Next we explore the rich parameter space provided by this model, by evaluating the web dynamics under the influence of changing web stiffness K_t, tension line stiffness K_r, and drag force coefficient C_w.

Slingshot spider dynamics as a function of web parameters (K_t, K_r, C_d)

Here we explore the effect of three parameters - radial stiffness K_r, tension line stiffness K_t and web drag C_w - on the dynamics of the slingshot motion. These parameters capture most of the mechanical and

Parameter	**Field data**	**Simulation 1**	**Rel. error %**	**Simulation 2**	**Rel. error %**
Rise time, t_r	9.48 ms	9.6 ms	1.25%	9.6 ms	1.25%
Peak, y_{max}	14.58 mm	15.07 mm	3.36%	14.81 mm	1.57%
Peak time, t_p	20.81 ms	20.25 ms	2.76%	20.5 ms	1.53%
Overshoot %	17.93 %	30.5 %	12.57%	23.89 %	5.96%
Settling time, t_s	37.84 ms	60 ms	58.5%	40 ms	5.71%

Table 2: **Comparison of simulation to single representative field data point** Summary of the spatiotemporal parameter outputs of simulations 1 and 2.

geometrical characteristics of the web and dictate the significant dynamics of the system. Simulations are performed by changing one of these parameters while keeping the others constant. For a convenient physical interpretation, we normalize the output displacements by the spider body length (BL) while using the results and parameters ($K_{t,ss}$, $K_{r,ss}$ and $C_{w,ss}$) from Simulation 2 as a reference. We showcase the resulting normalized displacement curves with respect to the reference plot in Fig. 6 and compare the sensitivity of the model outputs in terms of the aforementioned spatiotemporal parameters in Fig. 7.

Fig. 6a shows the normalized displacement curves when the radial line's stiffness K_r is changed while everything else remains the same. We observe that, for an order of magnitude decrease in the value of K_r, the web loses it's ability to oscillate and slowly asymptotes to the equilibrium point. This is similar to an overdamped system where drag dissipation dominates. Increasing $K_{r,ss}$ causes a faster rise in the displacement as well as a larger overshoot. These results are quantified in Fig. 7 which shows that as the radial stiffness increases, the spider travels a longer distance in a shorter time duration and takes a shorter time to settle. We (and others (Coddington, 1986; Eberhard, 1986)) have observed that slingshot spiders fire their webs in response to external vibratory/sound clues (finger snapping). It is therefore possible that spiders could release their webs in response to the nearby frequency of an insect's wing beat. Furthermore, it is key that the spider resets its web rapidly, as to not miss out on potential prey. Our model reveals that the slingshot K_r appears to balance finite overshoot at smaller peak and settle times, which could facilitate reaching a flying prey at a distance quickly, with minimizing oscillations to reset, and repeat motion if unsuccessful.

From the biomechanics context of the slingshot spiders motion, what does it mean to change parameters such as the stiffness of the radial lines? Stiffness depends on intrinsic molecular and geometric properties and is defined as $K_r = \frac{N_r E_r A_r}{L_{r,eq}}$. These properties vary among different species of spiders, and have never been measured specifically for *Epeirotypus* sp.. However, the young's modulus ranges between 1-10$\times 10^9$ Pa in the literature, depending upon external mechanical conditions such as such as strain, strain rate and environmental conditions such as temperature and humidity (Agnarsson et al., 2009; Su and Buehler, 2016; Yazawa et al., 2020). Another strategy to modify the radial stiffness would be changing by other geometrical parameters such as the equilibrium length $L_{r,eq}$ or the area A_r. For example Eberhard reports direct observations of *Epeirotypus* sp. using its legs to adjust the tension in the radial and sticky lines (by effectively changing $L_{r,eq}$) during web construction (Eberhard, 1981).

Next, we examine the role of the tension line highlighted in Fig. 6b. Since the tension line is not originally stretched ($\Delta L_t < L_{t,eq}$), varying the tension line stiffness does not affect the rise time $t_s \approx 10$ ms. Beyond this point, the tension line is engaged and applies a pulling force on the spider. In the limit of no tension line ($K_t = 0$), the system overshoots to almost two spider BL above the equilibrium point before slowly oscillating back to equilibrium. As the stiffness of tension increases, the overshoot decreases while the undershoot increases. For instance, at 10 $K_{t,ss}$, the maximum displacement decreases to less than one body length above the equilibrium before bouncing into almost two body lengths below the equilibrium point. This is due to the fact that at slightly above equilibrium, the time scale is mostly determined by the properties of the tension line, namely $t = \frac{2\pi}{\omega_{nd}} \sim \sqrt{\frac{m_s}{K_t}}$. Fig. 7b summarizes these results showing a monotonic decrease from 30% to almost 8% across four order of magnitudes in K_t. Meanwhile, the peak time is not as strongly influenced,

decreasing by only $\sim 10\ ms$ over four order span in K_t. Interestingly, we observe a minimum of around 40 ms near the reference value in the settling time due to the increase in the undershoot as K_t increases.

From a biomechanics context, our model suggests that, besides allowing the spider to load elastic energy and keep the web in static equilibrium, the tension line also plays an integral role during the slingshot motion. Without a tension line, the slingshot spider is completely at the mercy of air drag near the equilibrium point as radial forces become negligible due to geometry (see SI text Fig. 2). The tension line stiffness assists in preventing too much overshoot while decreasing the settling time. Controlling the overshoot and settling the web faster may allow the spider to reach the insect in its web faster. It may also reduce the time to reset and repeat its hunting motion in case of a missed prey capture. The tension line also allows the spider to control its vertical displacement at intermediate tension line lengths actively as observed in field experiments (See SI Movie 2).

Finally, we look at the effect of the web drag on the slingshot dynamics. Compared to the other two parameters, we observe that the model is highly sensitive to the drag coefficient.At a high damping coefficient (2 to 10$\times C_{w,ss}$), the system goes rapidly to an overdamped regime whereby the system gradually approaches equilibrium without any oscillations. At lower damping coefficient (0.1 to 0.5$\times C_{w,ss}$), the system becomes highly underdamped and vibrates with several body lengths around the equilibrium point. This is further highlighted in Fig. 7c, which shows that overshoot may reach up to 60% at 0.01 $C_{w,ss}$. At values larger than 10 $C_{w,ss}$, the overshoot is minimal or even non existent. The high sensitivity of the model to damping may be further exemplified in the settling time which shows a minimum near the reference value $C_{w,ss}$. Above the minimum value, the system is overdamped and takes a long time to reach the $\pm$ 1BL envelope around equilibrium. Below that minimum, the system becomes highly underdamped and fluctuates with high amplitudes around equilibrium.

Limitations of the model and future work

Our work aims to provide a reduced-order approach to modeling the complex dynamics in slingshot spider webs. However, we make certain assumptions in our model that can be further improved in future work.

Dissipation due to aerodynamic drag and molecular friction

Our model shows that aerodynamic drag at an intermediate to low Reynolds number adequately describes the damping experienced by the spider and its web. The model ignores the possible contribution of viscous dissipation within the viscoelastic spider threads. The relative effect of these two sources of dissipation in oscillating spider webs is underexplored and still an active area of research. Past work highlighted the importance of aerodynamic drag in the context of "ballooning spiders" (Sheldon et al., 2017; Suter, 1992) and the stopping of flying insects by orb weavers webs (Kelly et al., 2011; Sensenig et al., 2012). Other work however completely dismissed aerodynamic drag and attributed dissipation primarily to internal viscous damping (Aoyanagi and Okumura, 2010; Ko, 2004). A summary of studies exploring the role of dissipation, internal and external, is provided in SI Table 1.

Owing to the fineness of spider silk having a diameter $< 4\ \mu m$ (Ko, 2004), the characterization of the mechanical properties of the spider silk had been mainly experimentally limited to tensiometry or impulsive loading at lower strain rates. Replicating the high strain rates faced by the webs of the slingshot spiders studied in this work ($> 60\ s^{-1}$) is experimentally challenging. In addition, the mechanical properties and structural geometries of spiders' web silk are highly dependent on environmental conditions such as temperature, humidity, wind conditions, water content (supercontractility) and surrounding conditions such as the location and flexibility of the substrate (Gosline et al., 1999). This poses further difficulties in replicating the native conditions of spiders to experimentally examine the mechanical properties of the spider silk. Overall, our model reveals that viscous damping (in silk) is not necessary to capture the underdamped behaviour in the slingshot spider, but it could still be important and will be focus of future work (See SI text fig. 3).

Geometrical constraints

Our simulations also assume no coupling between the parameters. For instance, orb webs vary tremendously across species in the numbers of radii and rows of capture spirals (Craig, 1987; Sensenig et al., 2010)), but

slingshot spider webs are relatively similar to one another in having relatively few radii and around ten rows of capture silk in their webs (Eberhard, 1986). This might suggest geometric constraints on slingshot spider web topology and dimensions. Thus, this model may be extended to examine other web topologies and silk dimensions to test the hypothesis that the evolution of theridiosomatid web architecture is limited in part by optimizing the amount of aerial damping during the slingshot motion

Conclusion

We develop a 2D mathematical model to simulate the dynamics of the slingshot spider powered by its conical web geometry and tension line. We validate the model with experimental results and explore the sensitivity of various physical parameters governing web forces. We find that web parameters are finely-tuned to yield an underdamped oscillating web, that enables the spider to displace finite distances quickly, while minimizing residual oscillations in the web. These design parameters may enable the spider to exploit a risky hunting strategy of catching flying insects in mid-air while minimizing oscillations in its web due to its rapid movements. At the same time, the spider should be able to sense the vibrations induced by the flying preys and discern them from possibly faulty ones induced by the surrounding ambient air (Craig et al., 1985; Eberhard, 1981). Though we have presented a first approach for understanding this fascinating slingshot spider dynamics, open questions remain about the molecular structure of the radial silk and tension line, as well as their 3D-web topology that enables their agile power packed performance. These research questions open up rich avenues for multidisciplinary research, while furthering our knowledge and appreciation of arachnids and their ingenious engineering strategies for locomotion and survival.

Declarations

Funding

S.J. acknowledges funding support from the NSF under grant no. CBET-2002714. M.S.B acknowledges funding support through NSF award number 1817334 and CAREER 1941933 and National Geographic Foundation (NGS-57996R-19). T.A.B. acknowledges funding support from the NSF (IOS-1656645)

Conflicts of interest

The authors declare no competing interests.

Availability of data and material

All Matlab codes and data for this article are accessible here: `https://github.com/bhamla-lab/slingshotspider2021`

Ethics approval

All applicable international, national, and institutional guidelines for the care and use of animals were followed.

Author's contribution

SA, MSB collected field data. EJC, SA, SJ developed mathematical model. EJC, SA and SH analyzed data. EJC conducted simulations. All authors contributed to editing, interpreting and writing the manuscript. TAB, SJ and MSB managed funding and resources.

Acknowledgements We thank Jaime Navarro for his excellent field guide services in the Peruvian Amazon Rainforest.

References

Agnarsson I, Dhinojwala A, Sahni V, Blackledge TA (2009) Spider silk as a novel high performance biomimetic muscle driven by humidity. The Journal of experimental biology 212(Pt 13):1990–1994

Alexander SLM, Bhamla MS (2020) Ultrafast launch of slingshot spiders using conical silk webs. Current biology: CB 30(16):R928–R929

Alves DdA, Pioker FC, Ré-Jorge L, do Nascimento SM (2007) Funcoes do compartamento disparo da teia de naatlo sp.(aranea), theridiosomatidae. Ecologia da mata Atlantica

Aoyanagi Y, Okumura K (2010) Simple model for the mechanics of spider webs. Phys Rev Lett 104:038102

Coddington JA (1986) The genera of the spider family theridiosomatidae. Smithson Contrib Zool

Coddington JA (2005) Theridiosomatidae. Spiders of North America: an identification manual

Craig CL (1987) The ecological and evolutionary interdependence between web architecture and web silk spun by orb web weaving spiders. Biological Journal of the Linnean Society 30(2):135–162

Craig CL, Okubo A, Andreasen V (1985) Effect of spider orb-web and insect oscillations on prey interception. Journal of theoretical biology 115(2):201–211

Das R, Kumar A, Patel A, Vijay S, Saurabh S, Kumar N (2017) Biomechanical characterization of spider webs

Eberhard WG (1981) Construction behaviour and the distribution of tensions in orb webs. Bulletin of the British Arachnological Society 5(5):189–204

Eberhard WG (1986) Ontogenetic changes in the web of epeirotypus sp. (araneae, theridiosomatidae). The Journal of arachnology 14(1):125–128

Eberhard WG (1990) Function and phylogeny of spider webs. Annual review of ecology and systematics 21(1):341–372

Gary Leal L (2007) Advanced Transport Phenomena: Fluid Mechanics and Convective Transport Processes. Cambridge University Press

Gosline JM, Denny MW, DeMont ME (1984) Spider silk as rubber. Nature 309(5968):551–552

Gosline JM, DeMont ME, Denny MW (1986) The structure and properties of spider silk. Endeavour 10(1):37–43

Gosline JM, Guerette PA, Ortlepp CS, Savage KN (1999) The mechanical design of spider silks: from fibroin sequence to mechanical function. The Journal of experimental biology 202(Pt 23):3295–3303

Han SI, Astley HC, Maksuta DD, Blackledge TA (2019) External power amplification drives prey capture in a spider web. Proceedings of the National Academy of Sciences of the United States of America 116(24):12060–12065

Hingston RWG (1932) A Naturalist in the Guiana Forest. Longmans, Green

Jung S, Clanet C, Bush JW (2014) Capillary instability on an elastic helix. Soft matter 10(18):3225–3228

Kelly SP, Sensenig A, Lorentz KA, Blackledge TA (2011) Damping capacity is evolutionarily conserved in the radial silk of orb-weaving spiders. Zoology 114(4):233–238

Ko FK (2004) Engineering Properties of Spider Silk Fibers, Springer US, Boston, MA, pp 27–49

Ko FK, Kawabata S, Inoue M, Niwa M, Fossey S, Song JW (2011) Engineering properties of spider silk. MRS Online Proceedings Library 10.1557/PROC-702-U1.4.1

Kuo BC (1987) Automatic Control Systems, 5th edn. Prentice Hall PTR, USA

Sensenig A, Agnarsson I, Blackledge TA (2010) Behavioural and biomaterial coevolution in spider orb webs. Journal of Evolutionary Biology 23(9):1839–1856

Sensenig AT, Lorentz KA, Kelly SP, Blackledge TA (2012) Spider orb webs rely on radial threads to absorb prey kinetic energy. J R Soc Interface 9(73):1880–1891

Sheldon KS, Zhao L, Chuang A, Panayotova IN, Miller LA, Bourouiba L (2017) Revisiting the Physics of Spider Ballooning. Composites Part A: Applied Science and Manufacturing Women in Mathematical Biology pp 163–178

Su I, Buehler MJ (2016) Spider silk: Dynamic mechanics. Nature materials 15(10):1054–1055

Suter RB (1992) Ballooning: Data from spiders in freefall indicate the importance of posture. The Journal of Arachnology 20(2):107–113

Tietsch V, Alencastre J, Witte H, Torres FG (2016) Exploring the shock response of spider webs. J Mech Behav Biomed Mater 56:1–5

Vogel S (2009) Glimpses of Creatures in Their Physical Worlds. Princeton University Press

Wienskoski E (2010) The genus naatlo (araneae: Theridiosomatidae): distribution and taxonomic history. Revista Brasileira de Biociências 8(2)

Yazawa K, Malay AD, Masunaga H, Norma-Rashid Y, Numata K (2020) Simultaneous effect of strain rate and humidity on the structure and mechanical behavior of spider silk. Communications Materials 1(1):10

Yu H, Yang J, Sun Y (2015) Energy absorption of spider orb webs during prey capture: A mechanical analysis. J Bionic Eng 12(3):453–463

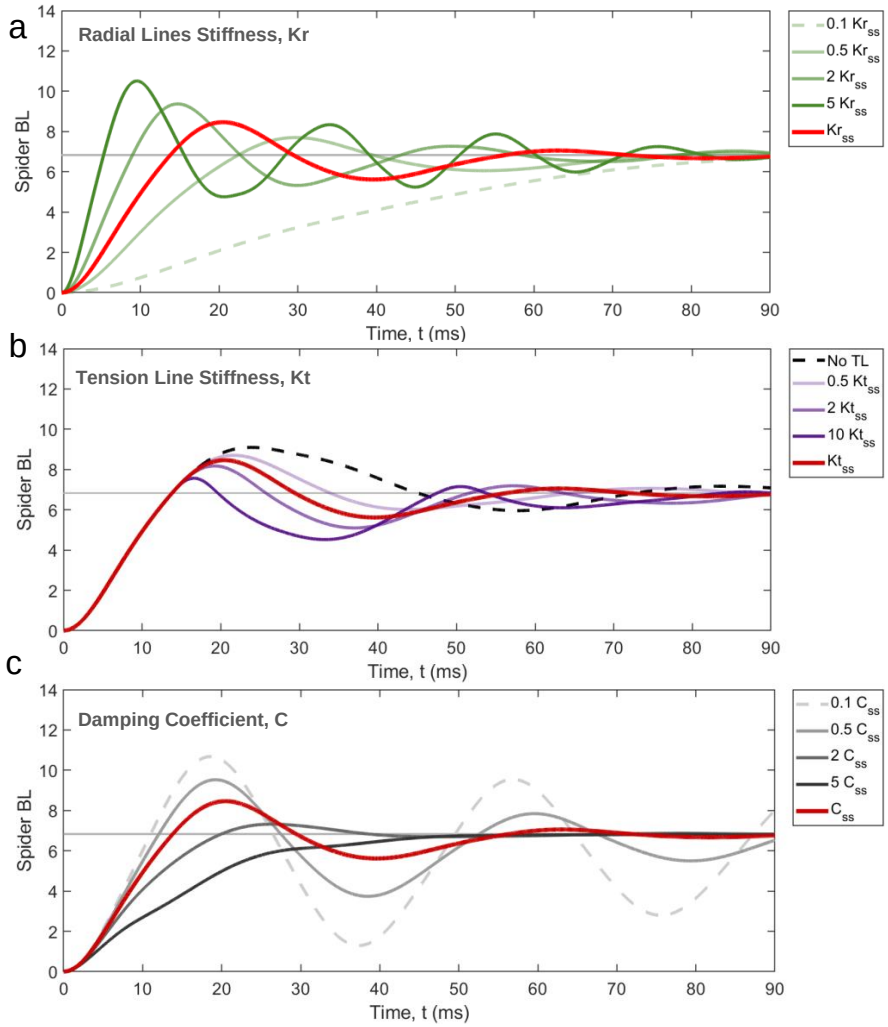


Fig. 6: **Exploring web dynamics as a function of model parameters.** We explore the impact of the different forces on the slingshot dynamics obtained from Simulation 2. The output displacements are normalized by the spider body length (BL) and parameters ($K_{r,ss}$, $K_{r,ss}$ and $C_{w,ss}$) from Simulation 2 (Fig. 5a) as a reference. **a** Increasing the radial lines stiffness K_r leads to both a faster increase in the initial displacement as well as higher overshoots (∼4 BL above equilibrium) with subsequent increasingly large amplitude vibrations around the equilibrium point. An order of magnitude decrease in the radial lines stiffness causes the system to slowly approach the equilibrium point without any observable overshoot. **b** Changing the tension line stiffness K_t only affects the dynamics past the equilibrium line. Without any tension force the system achieves a higher overshoot and more subsequent vibrations. As the tension line stiffness increases, the vibrations peaks become sharper above the equilibrium with larger and slower undershoot. **c.** The model reveals high sensitivity to web drag C_w. Halving the damping coefficient causes the system to significantly vibrate over two body lengths around the equilibrium line. Doubling the damping coefficient leads to a small overshoot as the system quickly approaches equilibrium without any noticeable oscillations, similar to critically damped oscillator.

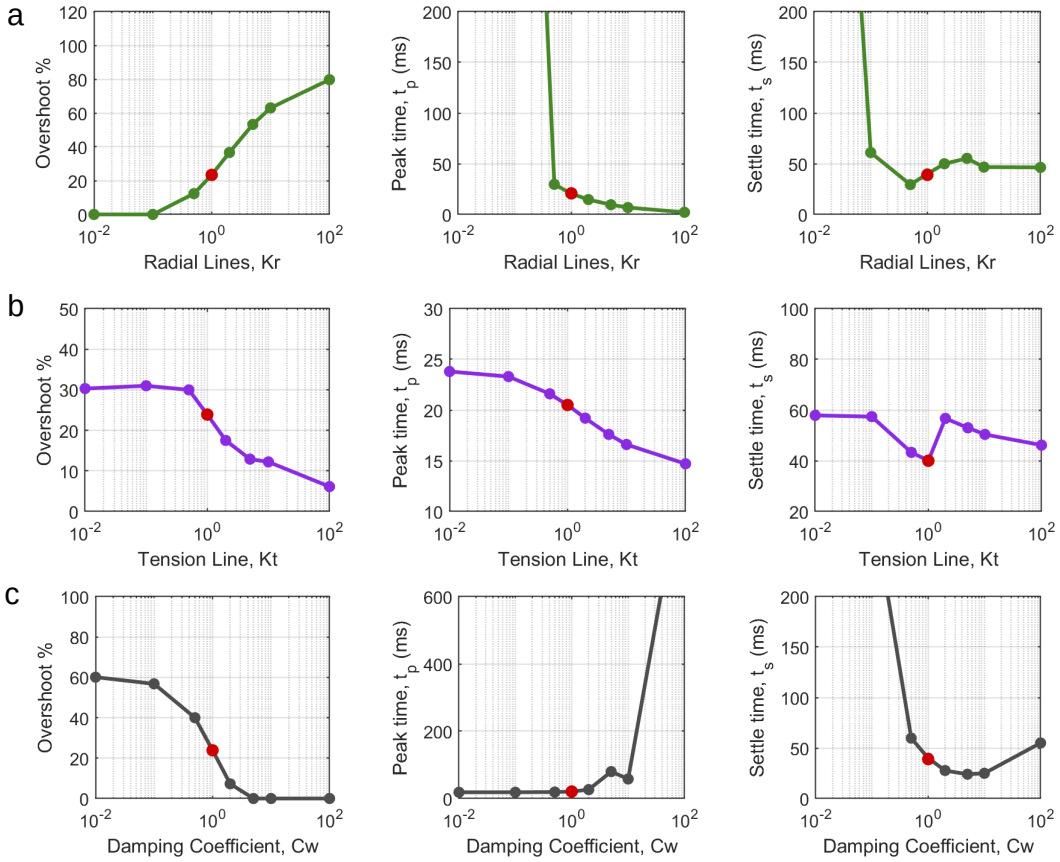


Fig. 7: **Summary of web dynamics as a function of model parameters.** We quantify the changes of the various simulations by focusing on the percentage overshoot, peak time (t_p) and settling time (t_s). We highlight the reference values in red **a.** The overshoot increases monotonically from 0 (no peak) to 80 % with the increase in $K_{r,ss}$. At low $K_{r,ss}$, the system does not vibrate around the equilibrium point causing t_p and t_s to go beyond the max simulation time of 200 ms. This behavior is tantamount to an overdamped dynamical system as the damping forces overcome the spring forces causing the . **b.** The overshoot decreases by almost 35% as K_t increases from 0.01 to 100 $\times$ K_t. Similarly, the peak time t_p slightly decreases from 24 ms to 15 ms as K_t increases. Interestingly, the settling time (t_s) decreases to a minimum of 40 ms around the reference value of K_t before sharply increasing. This is mainly due to the larger undershoot causes by a higher K_t **c.** The simulation is highly sensitive to the damping coefficient. The overshoot decreases from around 60% to almost no overshoot as damping increases. The settling time shows a minimum around the reference point as low drag causes the system to oscillate violently around the equilibrium point while a high drag causes it to slowly approach the equilibrium. Both effects yield an increase in the settling time.